Available online at www.sciencedirect.com

ScienceDirect

Procedia Structural Integrity 2 (2016) 1285–1294

Structural Integrity Procedia

www.elsevier.com/locate/procedia

21st European Conference on Fracture, ECF21, 20-24 June 2016, Catania, Italy

Investigation of the Effect of Internal Pores Distribution on the Elastic Properties of Closed-Cell Aluminum Foam: A Comparison with Cancellous Bone

M. J. Mirzaali[a,*], F. Libonati[a], P. Vena[b], V. Mussi[c], L. Vergani[a], M. Strano[a]

[a]*Department of Mechanical Engineering, Politecnico di Milano, Via La Masa 1, Milano 20156, Italy*
[b]*Department of Chemistry, Materials and Chemical Engineering "G. Natta", Politecnico di Milano, Via La Masa 1, Milano 20156, Italy*
[c]*Machine Tools and Production Systems-MUSP Laboratory, Via Tirotti 9, Piacenza 29122, Italy*

Abstract

Closed-cell aluminum foams belong to the class of cellular solid materials, which have wide application in automotive and aerospace industries. Improving the mechanical properties and modifying the manufacturing process of such materials is always on demand. It has been shown that the mechanical properties of cellular materials are highly depending on geometrical arrangement, mechanical properties of solid constituents and the relative density of these materials. In this study, using a manufacturing process of foaming by expansion of a blowing agent, we prepared two types of closed-cell aluminum foams with isotropic distribution of cells along length and foams with gradient of pores along its length. We hypothesized that such variation of pores can induce microstructural directionality along the length of foam samples and improve their mechanical properties. For this aim, we studied the microstructural properties by micro-CT imaging and found their relation to macroscopic mechanical properties of foam samples by conducting monotonic compression tests. We compared these results with the one of the bovine femur trabecular bone as they show a dominant microstructural anisotropy due to alignment with the maximum strength direction in body. We also conducted numerical analyses and validated them for the elastic part based on our experimental work.

Our results showed that gradient variation in porosity in closed-cell aluminum foams have a minor effect on their macroscopic mechanical properties. Although using such materials in sandwich panel structures, the strength of the material slightly increased. In addition, parameters of a power law model for the description of mechanical properties of foam sample and their relative density and properties of the solid compartment were characterized. The presented results are considered as a preliminary study for improvement of mechanical properties of closed-cell aluminum foams.

Copyright © 2016 The Authors. Published by Elsevier B.V. This is an open access article under the CC BY-NC-ND license (http://creativecommons.org/licenses/by-nc-nd/4.0/).
Peer-review under responsibility of the Scientific Committee of ECF21.

Keywords:
Closed-cell Aluminum Foam; Bio-inspiration; Microstructural Anisotropy, Finite Element Modeling, Computed Tomography.

* Corresponding author. Tel.: +39-022-399-8203 ; fax: +39-022-399-8263.
E-mail address: mirzaalimazandarani.mohammad@polimi.it

Copyright © 2016 The Authors. Published by Elsevier B.V. This is an open access article under the CC BY-NC-ND license (http://creativecommons.org/licenses/by-nc-nd/4.0/).
Peer review under responsibility of the Scientific Committee of ECF21.
10.1016/j.prostr.2016.06.164

1. Introduction

Closed-cell and open-cell foams, honeycombs with periodically repeating 2D or 3D unit cells, and sandwich panels are examples of cellular solid materials, which have various application in engineering structures, such as automotive and aerospace industry (Degischer et al., 2013). From the mechanical point of view, these materials can be used in the load-bearing parts of structures which require the high capability of energy absorption with less weight (Ashby et al., 2000). They also have functional applications in cases where interconnected porosity is required, for instance in the production of biomedical implants and scaffolds (Gibson et al., 2010).

Cellular solid materials can also be found in nature, such as trabecular bone, cork, sponges, and wood. Because of their unique combination of strength and toughness with high energy absorption capability, cellular materials in nature can be considered as a source of inspiration for man-made products (Gibson et al., 2010; Wegst et al., 2015). Mimicking the microstructures of natural materials, with the aim of improving the mechanical properties of the artificial products was hot trend over the two decades. A density-graded cellular aluminum is an example of producing artificial material with the aim of improving mass-efficiency in load-bearing structures (Brothers and Dunand, 2006). Mimicking the mechanical and microstructural features of cellular materials, such as trabecular bone, is crucial in the medical science, to prevent stress shielding of bone implants and to improve the biological fixation and integration of implants (Mottassi et al., 2013; Gibson et al., 2010). Another aim of such mimicking was to determine whether cellular materials such as foams might be suitable as mechanical models of trabecular bones in biomechanical applications (Guillén et al., 2011).

Among natural materials, trabecular bones are heterogeneous highly porous composite materials made of protein and mineral with different hierarchical levels (Keaveny et al., 2001). Trabecular bones are made up of a three-dimensional network of plates and rods and can be best described by open-cell foams (Gibson et al., 2010). The mechanical properties of foams and trabecular bones depend not only on the mechanical properties of solid itself but also on the amount of this material and the geometrical arrangement of the structure (Gibson, 2005). It has been shown that the apparent density, which is the apparent weight to apparent volume ratio, is the most important factor affecting and describing the mechanical properties of trabecular bone (Rietbergen et al., 1998; Rincón-Kohli, 2003), and synthetic foams (Patel, 1969). Mechanical properties of cellular solid also depend on the architecture, and the orientation of the microstructures in both trabecular (Goulet et al., 1994; Turner et al., 1990; Goldstein et al., 1993) and synthetic foams.

Our aim in this study is to implement our current rapid and inexpensive manufacturing process for the production of closed-cell aluminum foams with the improved mechanical properties. For the improvement of the mechanical properties of such materials, we followed the loading adaptation of the trabecular bones. Based on Wolff's law (Wolff, 1986; Frost, 1994) the trabecular microstructure is typically oriented along the maximum load (principal stress) directions. This microstructural directionality will result in anisotropy of mechanical properties in trabecular bone. Based on this fact, we tried to introduce a variation of pores in the microstructural configuration of a closed-cell aluminum foam in order to induce some sort of directionality inside the foam samples. We hypothesized that such directionality will improve the mechanical properties of foam cells compared to the case that pores are homogeneously distributed. For this aim, we produced two types of aluminum closed-cell foams with homogeneous and graded distribution of pores, and investigated such effects on the mechanical properties of the foam samples. These results were also compared with the mechanical properties of the trabecular bones in the literature. Using micro-computed tomography (μCT), 3D representations of the microstructures of foam materials were analyzed, and well-known morphological parameters were obtained. The Effect of the microstructures on the macroscopic mechanical properties of foam materials was analyzed and our results were compared with the empirical formulas of foam and bone materials. Finally, a micro-finite element (μFE) model was build from μCT images and validated for the estimation of elastic properties of foam materials. An elastic perfectly plastic material model was implemented in the FE-model to predict the post-yield behavior of foam materials under compression loading, and a comparison between numerical and experimental results were performed.

Nomenclature

C	elastic modulus

$\Sigma_{y0.2}$	yield stress
$E_{y0.2}$	yield strain
Σ_{ult}	strength
E_{ult}	ultimate strain
Tb.Th	trabecular (strut) thickness
Tb.Sp	trabecular (strut) spacing
ρ_s	relative density
ρ_p	porosity
μCT	micro-computed tomography

2. Material and Method

2.1. Sample preparation

Aluminum foam specimens were prepared using the well-known powder compact foaming technique in which a mixture of powders containing AlMg1Si0.6 composition with a 0.8 %wt of TiH_2 as blowing agent are compacted to a dense commercial precursor (Mepura ™) and foamed above the melting temperature of the resulting alloy (Banhart, 2001; Baumgrtner et al., 2000). Precursor rods with 10 mm in diameter were cut by band-saw and the sawed surfaces were ground with a sand paper (120 grit SiC) to obtain cylinders weighed at $2.99 \pm 2\%\ g$.

A single precursor was inserted into a cylindrical foaming mold, made of a titanium tube, with an inner diameter of 10.9 mm and 0.8 mm thickness. Two stainless steel end caps (14 mm thickness) were put at both ends in order to limit foam expansion to the desired final length of about 50 mm. The inner volume of the mold was chosen in order to produce foamed specimens with an overall density of 650 $\frac{kg}{m^3}$ from a 2.99 g precursor cylinder. Two different precursor layouts were used during this work. In order to have a homogeneous distribution of foam cells, precursors were placed in the middle of the die. Density variation in pores were obtained by placing the precursors close to one end.

The mold was placed at the center of an air convection laboratory furnace (Nabertherm L9/11-HA) and preheated at 750°C for about 205 s. In order to achieve the best temperature uniformity during the heating and foaming phases, the mold support in the furnace was designed with only four contact points with the foaming mold to minimize the amount of heat exchanged by conduction.

The mold was then extracted, positioned on a cooling support, rotated 360° around its longitudinal axis in the steady air and finally cooled with compressed air to the ambient temperature.

Seven closed-cell aluminum foam samples with graded distribution of pores and seven samples with homogeneous distribution of pores were analyzed in this study. Foam samples had an initial length of about 50 mm and diameter of about 10.5 mm. A lathe turning machine was used to remove about 1.5 mm of the outer skin of the five foam samples of each group. Damaged parts of the specimens due to milling have been cut by a circular blade saw (abrasive cutting instrument, HITECH EUROPE) with constant water irritation and finally, cylindrical specimens with the diameter of 9.5 mm and length of 18 mm were prepared. Aluminum foams are divided into the following groups, and illustrated schematically in Fig. 1:

- Group A: homogeneous cells distribution, with boundary skin (Number of specimens: 2)
- Group B: homogeneous cells distribution, without boundary skin (Number of specimens: 5)
- Group C: graded distribution of pores, with boundary skin (Number of specimens: 2)
- Group D: graded distribution of pores, without boundary skin (Number of specimens: 5)

For comparison of foam materials with trabecular bones, thirteen trabecular specimens were included in this study. Cancellous bone samples were harvested from the lower extremity of the bovine femur. Samples were drilled using a coring device (WÜRTH MACHINERY) in the principal direction of the trabecular structures. The coring device has the inside diameter of 10 mm and length of 30 mm. Subsequently, the samples were transferred to a lathing machine (OPTIMUM) to reduce them to cylinders with the diameter of 8 mm and height of 26 mm. During the drilling

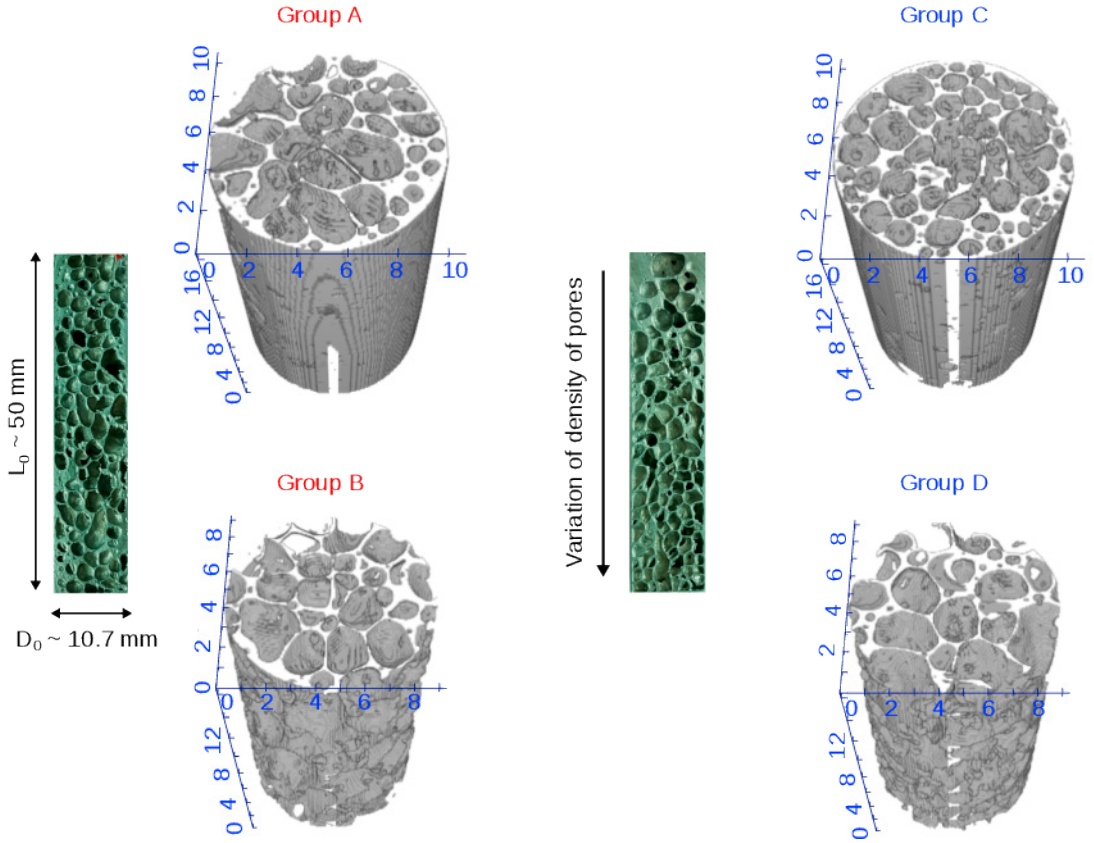

Fig. 1. A longitudinal cross-section of aluminum foam material is shown in the first and the third columns. μCT images of the cut specimen were shown in the second and the fourth columns. Dimensions in the image are in mm. Specimens were divided into four groups; Group A: homogeneous distribution of cells with skin, Group B: homogeneous distribution of cells without skin, Group C: graded distribution of cells, with skin, Group D: graded distribution of cells without skin.

and milling, specimens were kept wet by water. The trabecular cylinders were dried for 24 h at room temperature. Afterward, to reduce the edge effects (Keaveny et al., 1997) and to allow a correct load transmission reducing the stress concentration at the grips, the end of the bone samples were glued in a custom-made aluminum end caps, using epoxy adhesive (LOCTITE 435 Instant Adhesive). The end caps had inside diameter of 8 mm and outside diameter of 10 mm and covered 7 mm of the bone specimens. The outer side of the bone samples, as well as the aluminum tubes, were defatted using acetone before gluing. Custom-made alignment tools were used to keep the bone and end caps aligned with the direction of axial loading.

2.2. *Micro-CT image analysis*

Micro-computed tomography (μCT) images of the foam and bone samples have been collected using an x-view scanning equipment (North Star Imaging Inc.) with the spatial resolution of 20 μm, and 27 μm, respectively. Parameters of the scanning were fixed at 40 kV and 220 μA for aluminum samples and 112 kV and 21 μA for bone specimens. Simultaneously, five foam specimens were placed in the CT equipment. Scanning of the trabecular specimens was done in wet condition while the bone samples were submerged in saline solution (NaCl 0.9%). Total imaging time was approximately 25 minutes. Image reconstruction was performed by the x-view CT software. Image analysis has been done in ImageJ software (Abramoff et al., 2004) on the cylindrical region of interest (ROI) equal to the smallest diameter of foam/ trabecular samples in each group. Using a Gaussian blur filter (σ = 1.5), noises were removed from the images. Consequently, images were converted to gray-level 8-bit images. Otsu local thresholding method (Otsu, 1979) has been used for the segmentation of the images which resulted in binary images with the voxel

value of 1 for aluminum/ bone and 0 for the empty spaces. The porosity, ρ_p was defined as the total number of cavities to the total number of voxels in ROI in the binary image, and relative density, ρ_s is defined as $\rho_s = 1 - \rho_p$. Trabecular (strut) thickness (Tb.Th) and trabecular (strut) spacing (Tb.Sp) were calculated based on the conventional definition of the greatest sphere diameter that fits within the structure (Hildebrand and Rüegesegger, 1997; Doube et al., 2010). The strut thickness and strut spacing are related to foam microstructural features.

2.3. Compression testing

A quasi-static monotonic compression loading was conducted using an MTS machine (Alliance, RF/150) with the load cell of 150 kN (class 1 ISO 7500-1) and under the stroke rate of $8.5 \times 10^{-2}\ \frac{mm}{s}$ (strain rate of $5 \times 10^{-3}\ s^{-1}$) for testing the foam samples. The axial strain was measured using an MTS extensometer. Testing was conducted at room temperature and axial displacement (S), axial loading (F), time and axial strain (E) were recorded by the sampling rate of 20 Hz. Nominal stress (Σ) was defined as the ratio of axial force (F) to initial area (A_0) obtained from μCT scans for each sample. The yield stress ($\Sigma_{y0.2}$) and yield strain ($E_{y0.2}$) were obtained based on a 0.2% offset criterion. The elastic modulus (**C**) was calculated using a moving regression with a box width of 0.2% strain to identify the stiffest section of the loading part. The ultimate stress (Σ_{ult}) was obtained as the primary maximum stress before densification and its corresponding strain as ultimate strain (E_{ult}).

2.4. Finite element analysis

3D μFE models were generated from the geometry of the scanned specimens using the Gmsh software (Geuzaine and Remacle, 2009). Briefly, a prismatic cube with the ratio of 2:1 was cropped from CT images. Then, point clouds corresponding to the contours of the each specimen were extracted from the μCT image using isosurface module in bonej (Doube et al., 2010). Isolated pixels were removed using corresponding filters in MeshLab with setting the maximum diameter of 15 μm for removing the isolated pieces. The number of triangulation were reduced with the quadric edge collapse decimation filter in MeshLab (Cignoni et al., 2008) to have about 200,000 triangular faces. Self-interface surfaces were removed in geomagic software (GeomagicsDesingX, 2013). Second-order tetrahedral elements with frontal algorithm (Schoeberl, 1997) were used for 3D meshing in Gmsh, and finally, the mesh was optimized to improve the quality of tetrahedral elements. Each FE model had about 200,000 second-order tetrahedral elements and numerical analysis has been done in ABAQUS (Dassault Systmes, 2012). Isotropic elastic modulus of the individual elements in FE model were calibrated with respect to the experimental results to have similar macroscopic elastic modulus. Linear elastic- perfectly plastic material model was assumed for each element. Initial guess for the microscopic yield stress for each element was chosen from the specific strength, ($\frac{\Sigma_{ult}}{\rho_s}$), of the experimental compression tests.

Linear model and statistical analysis were performed in R (R Development Core Team, 2008), and $p < 0.05$ were assumed as the significant level for the t-tests.

3. Results

3.1. Morphology analysis

In this study, we included fourteen closed-cell aluminum foams, which were divided into four groups (A, B, C, and D). Samples in groups A and B had similar homogeneous cells distribution while an induced variation of pores size was considered in samples in groups C and D. The only difference between samples in group A(or C) and B (or D) is that the outer skin has been removed in samples of group B and D. The mean mass for the foam specimens was 2.94 g with the average density of 646.08 $\frac{kg}{m^3}$. The relative density of each specimen before cutting was physically measured. From this measurement, isotropic foams (Group A and B) showed the average relative density of 23.62 % and foam with directionality (Groups C and D) had a mean relative density of 24.23 %. Relative density calculated by image analysis were 19.8 % and 21.4 % for two samples in group A and 23.3 % and 21.7 % for two samples in group C. Due to the shorter specimens in groups A and C with respect to original samples, this difference in relative density is anticipatable.

Morphological parameters for the two other groups of closed-cell aluminum foam are presented in Table 1. No significant statistical difference was found between porosity of two groups ($p < 0.05$), although the mean value for the relative density of foam materials in group D (19.08 ± 2.14 %) show slightly higher value compared to relative density of group B (16.62 ± 1.7 %). Samples in group D exhibit slightly higher porosity. To increase the power of correlation of the mechanical and microstructural properties, we pooled results of relative densities of two groups (B and D).

Similar results were obtained for the other geometrical features such as the thickness of the strut and the spacing between the struts for foam materials. Comparing the relative density of foam specimens and bone samples, show that trabecular specimens in this study have higher relative density (34.14 ± 4.52 %).

Table 1. Morphological parameters calculated for foam and trabecular bone. Mean ± standard devision is presented in the table.

Specimen	Number of Specimen	ρ_s [%]	Tb. Th [μm]	Tb. Sp [μm]
Isotropic Foam (B)	5	16.62 ± 1.7	225.4 ± 7.02	1619 ± 152.6
Foam with Directionality (D)	5	19.08 ± 2.14	216.8 ± 10.5	1414 ± 93.6
Trabecular Bone	13	34.14 ± 4.52	209.7 ± 17.7	495.2 ± 48.76

3.2. Compression testing

Stress-strain curves of the monotonic compression testing are plotted in Fig. 3. All samples happen to follow similar behavior under compression loading and stress-strain curves can be divided into three major different regions; linear elastic deformation due to elastic cell bending till plastic yielding causes collapse of the cell wall, constant stress plateau due to progressive cell wall damage which produces breakage and buckling of the cells and inelastic region, densification due to the cell collapsing and contacting the cell wall which results in a steep stiffness increase (Gibson, 2005). Macroscopic mechanical properties of the mechanical tests for foam samples in groups B and D are sorted in Table 2. There were no significant difference between all mechanical properties of samples in groups B and D ($p < 0.05$), therefore these data were pooled. Comparing the macroscopic mechanical properties and intrinsic mechanical properties of foam material in both groups show a 5 to 6 times reduction in material properties. It has been shown by Gibson et al. (2010) that mechanical properties of open-cell foams can be estimated by Eq. 1, where X is mechanical properties of open-cell foam such as yield stress or elastic modulus, X_s is mechanical properties of solid cell wall material, and α_0 is a constant. For instance, for yield strength of an open-cell metal foam it is calculated as 0.3 (Gibson and Ashby, 1997). n is reported as 2 and 1.5 for the elastic modulus and plastic collapse strength of open-cell aluminum foams (Gibson et al., 2010). As a comparison, the parameter n is reported between 1.5 to 2 for human and bovine trabecular bones (Gibson et al., 2010; Keaveny et al., 2001), and between 0.7 to 2.6 for axial and torsional properties of human cortical bones (Mirzaali et al., 2015).

$$\frac{X}{X_s} = \alpha_0(\rho_s)^n \tag{1}$$

We calculated the parameter of n for the different mechanical properties of foam samples and found a significant correlation between macroscopic elastic modulus, strength and yield stress with the relative density of aluminum samples in two groups (pooled results, Fig. 2). Between elastic modulus and strength, strength property shows stronger correlation with the relative density ($p = 0.04$, $R^2 = 0.36$, $n = 1.23$) (Eq. 1).

No significant correlation was observed between yield strain and ultimate strain with relative density, and they show a constant value over relative density changes. Elastic modulus has no correlation with the strut thickness and strut spacing ($p < 0.05$). Strength results also show no correlation with strut spacing ($p < 0.05$), but a significant correlation found between strength and strut thickness ($p = 0.002$, $R^2 = 0.54$, $n = 2.4$). The presence of such a correlation could be because strut thickness itself is linearly correlated with relative density ($p = 0.04$, $R^2 = 0.25$).

The normalized stresses were plotted in Fig 3. The stresses were normalized to the relative density to the power of n of each foam sample. The parameter n is obtained from the power model of strength and relative density in

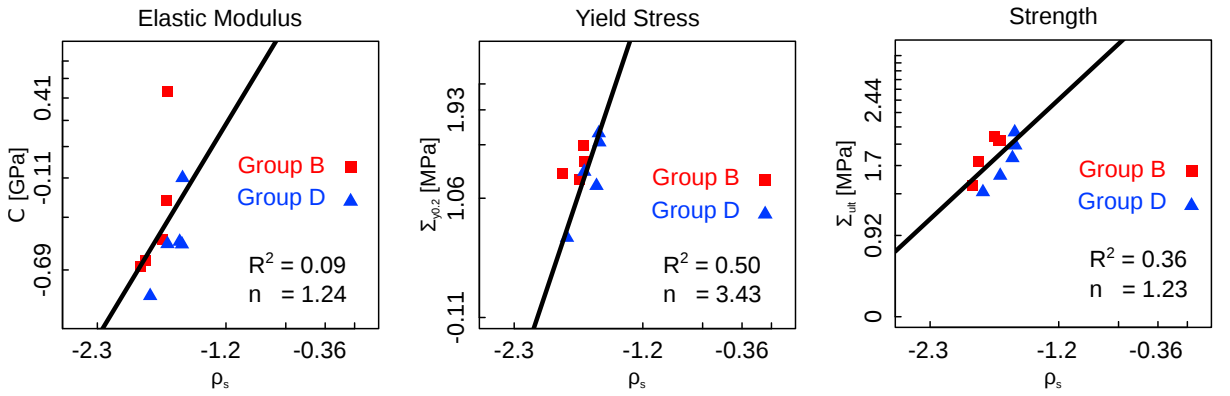

Fig. 2. Linear regression model in logarithmic scale for mechanical properties of closed-cell aluminum foams in groups B and D. Model is fitted to follow the power law presented in Eq. 1, to obtain the parameter n. Linear model is fitted on the pooled data (groups B and D. The parameter n for elastic stiffness and strength in open cell foam are reported as 2 and 1.5 (Gibson et al., 2010).

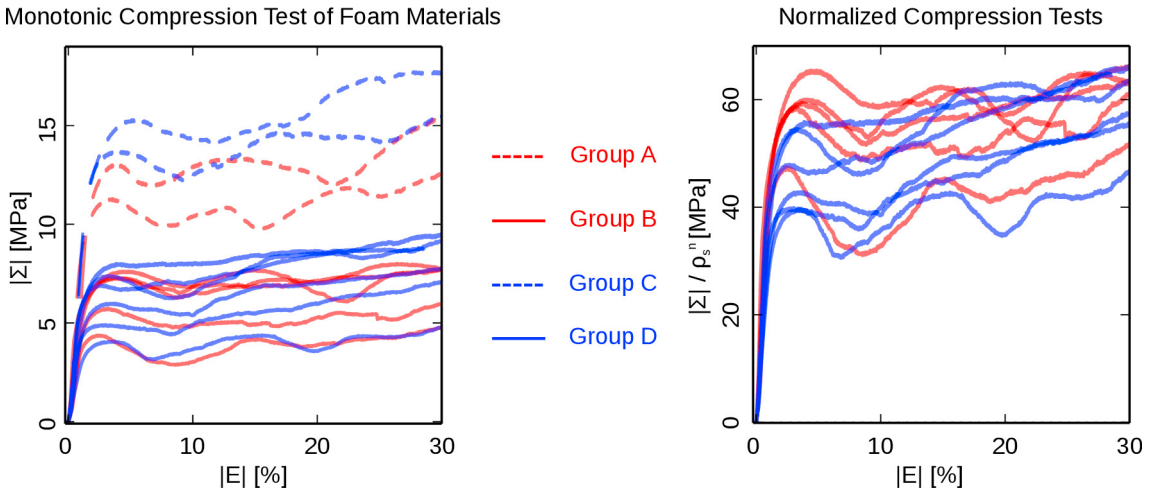

Fig. 3. Left: Monotonic stress-strain curve of monotonic compressive mechanical testing of closed-cell aluminum foam. Mechanical testing of 4 groups are compared to each other. Samples with skin in groups A and C show higher strength. There is no significant difference between mechanical behavior of samples in groups B and D. Right: Normalized stress-strain curves; stresses were normalized to ρ_s^n, where $n = 1.33$ is calculated by fitting a power law relation between compressive strength and relative density in Eq. 1 and Fig 2. Average strength of 40 MPa was used as initial guess for the perfectly plastic behavior in FE-model.

Fig 2. These results give an estimation of solid constituent of foam material without artificial voids. Mean ± standard devision for specific strength, ($\frac{\Sigma_{ult}}{\rho_s^n}$), were 58.24 ± 6.57 MPa for samples in group B and 45.29 ± 6.81 MPa for samples in group D. Mean of specific strength was taken as an initial guess for the elastoplastic finite element simulation of each group (Fig. 4). Specific elastic modulus, ($\frac{C}{\rho_s^n}$), for samples in group B and D were 7.19 ± 3.25 GPa and 4.79 ± 0.91 GPa, respectively.

Samples in groups A and C (with skin) show higher mechanical properties than samples in groups B and D. It is because of approximately 1.5 mm aluminum shells that covers those samples and produces a circumferential rigidity which leads to increase of the mechanical properties. From the rule of mixtures, we can assume that foam samples

Table 2. Mechanical properties of monotonic compression testing of closed-cell aluminum foam for the specimens in group B and D. Mean ± standard devision is presented in the table.

Specimen	**C** [GPa]	$\Sigma_{y0.2}$ [MPa]	$E_{y0.2}$ [$\frac{mm}{mm}$], %	Σ_{ult} [MPa]	E_{ult} [$\frac{mm}{mm}$], %
Isotropic Foam (B)	0.80 ± 0.44	3.38 ± 1.57	0.66 ± 0.24	6.47 ± 1.38	3.48 ± 0.82
Foam with Directionality (D)	0.62 ± 0.17	3.91 ± 1.41	0.83 ± 0.18	5.98 ± 1.56	3.30 ± 0.49

in group A and C are a combination of foams in groups B and D with a rigid circular cylinder with the thickness of 1.5 mm, and it can be predicted by Eq.2:

$$\Sigma = \frac{\sigma^F A_F + \sigma^* A_S}{A_F + A_S} \tag{2}$$

where Σ is the specific macroscopic strength/ yield properties, σ^F is microscopic strength/yield properties of foam, and σ^* is microscopic mechanical properties of solid section that contains skin. A_F is cross section area of foam sample, and A_S is the cross-section of the solid with cylindrical section and thickness of 1.5 mm that can be calculated exactly from μCT images. From the experimental results we can calculate the microscopic strength mechanical properties of the solid compartment. Considering average values of stresses as $\frac{\Sigma_{ult}}{\rho_s^n} = 88$ MPa and $\frac{\sigma^F_{ult}}{\rho_s^n} = 52$ MPa with the average cross-sectional areas as $A_F = 72.68\ mm^2$ and $A_S = 17.74\ mm^2$, the specific strength of the solid section, $\frac{\sigma^*_{ult}}{\rho_s^n}$ is equal to 236 MPa. These results are slightly higher than the range (97 to 172 MPa) compressive strength of Al6061, which is the closest material to its compartment. Assuming elastic modulus equal to 70 GPa for Al6061, the parameter $\alpha = 0.08$ can be estimated for Eq. 1.

Solid cell-wall properties of human trabecular bone are: compressive strength, $\sigma^*_{ult} = 182$ MPa, elastic modulus, equals to 18 GPa , with density of $\rho = 1800\ \frac{kg}{m^3}$.

3.3. FE simulation

For the μFE simulation, we defined a linear elastic-perfectly plastic material properties for each element. The geometrical nonlinearity was included in the analysis. A displacement-control boundary condition equal to 30 % of strain was applied on a reference point defined on top of the model and along the longitudinal axis of the specimen. A kinematic coupling was defined between the reference point and the upper surface of the specimen. A clamped boundary condition was set for the all nodes in the opposite side of the FE model. Macroscopic elastic stiffness calculated from experiments and numerical simulation are compared in Fig 4. Calibrated elastic modulus obtained from FE simulation were 5.85 ± 2.78 GPa and 4.83 ± 0.69 GPa for samples in group B and D, which is comparable with the specific elastic modulus calculated from experimental results.

Plastic stress limit was set to 45 MPa for the plastic simulation, which is calculated from specific strength results of the compression tests. Numerical and experimental results were compared in Fig. 4. Elasto-plastic FE model shows a reduction in stress after yielding. This model may only be used for the prediction of the initiation of yielding and is validated for the prediction of the elastic properties of the foam material. It is observed from the FE and experimental results that this model cannot properly follow the post-yield behavior of the material properly.

4. Conclusion

In this study, based on the loading adaptation of the trabecular microstructures, we proposed a new design for the closed-cell aluminum foam by inducing a density variation of pores inside such materials. We measured the microscopic geometrical properties of such foams using μCT imaging, and compared them with the ones of foams with homogeneous distribution of pores, and bovine trabecular bone. The monotonic compression tests were performed on two types of foam samples and the correlation of microscopic and macroscopic properties were investigated. From the experimental results, variation of pores along the foam materials does not have a major influence on the macroscopic

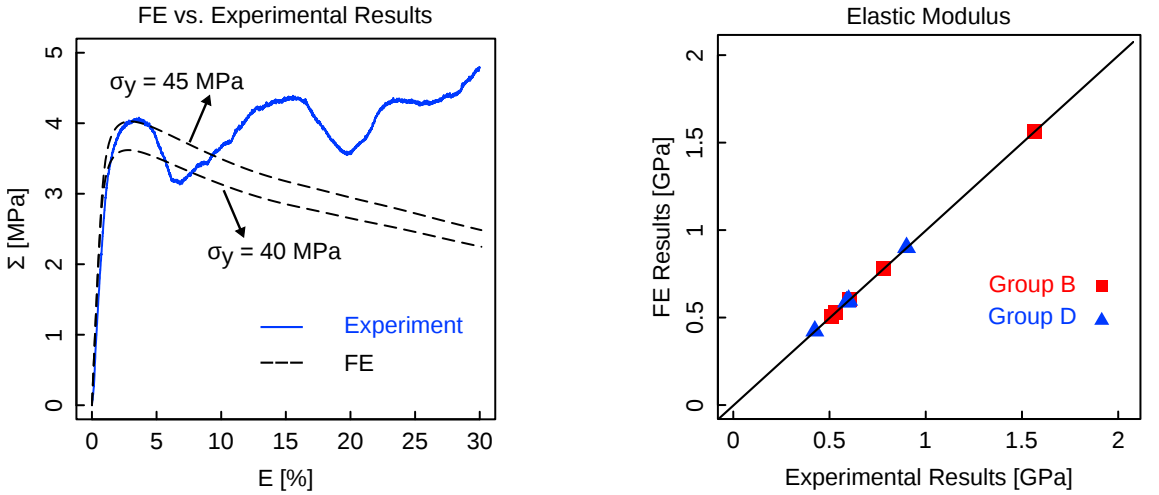

Fig. 4. Left: Experimental result belongs to the specimen of group D. FE simulation include a elasto-plastic model based, and two different microscopic yield stress were considered for the numerical simulation. Initial guess for the yield stress is based on specific strength in Fig 3. Right: Comparison of the macroscopic elastic modulus measured from experimental and numerical simulation. The solid line shows a one-to-one correlation of FE and experimental results.

mechanical properties of these materials and it is necessary to modify the manufacturing process in order to reach a significant microstructural anisotropy. From the experimental results, we found out that the relative density is a main predictor of the mechanical properties.

We were able to produce μFE models of μCT images. The Finite Element model was able to simulate the elastic response of the material samples for different relative density; it was also suitable to predict the first yielding. Therefore, this model can be used for the future parametric studies with the aim of obtaining a design guideline for the minimum mass. However, the stress strain relationship at large plastic strain was not correctly simulated. The numerical results can be improved by defining the rigid surfaces and contact instead of applying a load on the reference point coupled to the structures.

μFE model of trabecular bone can be created from μCT images, and validated by experimental results in similar fashion. This model can be used for the understanding of the failure mechanisms in the trabecular bones. This model can be compared with the ones of foams. It can also help us to find more features in the trabecular structures and implement them in the new design for foams. A limitation of this study is the small number of cohorts of foam samples and slight variation of their microstructural properties. Increasing the sample size variation may have an influence on parameters calculated in this study.

Acknowledgements

The authors would like to thank Dr. Stefano Petró for helping in μCT imaging, Lorenzo Giudici for helping in mechanical testing, and Luigi Baglioni and Dr. Tomaso Villa for bone sample preparation.

References

Abramoff, M., Magelhaes, P., Ram, S., 2004. Image processing with imagej. Biophotonics International 11, 36 – 42.

Ashby, M.F., Evans, A.G., Fleck, N.A., Gibson, L.J., Hutchinson, J.W., Wadley, H.N.G., 2000. Metal Foams: A Design Guide. Butterworth-Heinemann.

Banhart, J., 2001. Manufacture, characterisation and application of cellular metals and metal foams. Progress in Materials Science 46, 559 – 632.

Baumgrtner, F., Duarte, I., Banhart, J., 2000. Industrialization of powder compact toaming process. Advanced Engineering Materials 2, 168 – 174.

Brothers, A.H., Dunand, D.C., 2006. Density-graded cellular aluminum. Advance Engineering Materials 8, 805 – 809.

Cignoni, P., Callieri, M., Corsini, M., Dellepiane, M., Ganovelli, F., Ranzuglia, G., 2008. Meshlab: an open-source mesh processing tool, The Eurographics Association. pp. 129 – 136.

Dassault Systmes, 2012. Abaqus v6.12 DocumentationABAQUS Analysis User's Manual. ABAQUS Inc. ISBN 3-900051-07-0.

Degischer, H.P., Foroughi, B., Kottar, A., 2013. Metal Foams, Fundamental and Application. DEStech Publications, Inc.. chapter 4. pp. 97 – 127.

Doube, M., Kłosowski, M.M., Arganda-Carreras, I., P., C.F., Dougherty, R.P., Jackson, J.S., Schmid, B., Hutchinson, J.R., Shefelbine, S.J., 2010. BoneJ: Free and extensible bone image analysis in ImageJ. Bone 47, 1076 – 1079.

Frost, H.M., 1994. Wolff's law and bone's structural adaptations to mechanical usage: an overview for clinicians. The Angle Orthodontist 64, 175 – 188.

GeomagicsDesingX, 2013. User Guide, Geomagics XOS. 3D Systems, Inc.

Geuzaine, C., Remacle, J.F., 2009. Gmsh: A 3-d finite element mesh generator with built-in pre- andpost-processing facilities. International Journal for Numerical Methods in Engineering 79, 1309 – 1331.

Gibson, L.J., 2005. Biomechanics of cellular solids. Journal of Biomechanics 38, 377 – 399.

Gibson, L.J., Ashby, M.F., 1997. Cellular solids: Structure and properties. Cambridge: Cambridge University Press .

Gibson, L.J., Ashby, M.F., Harley, B.A., 2010. Cellular Materials in Nature and Medicine. Cambridge University Express.

Goldstein, S.A., Goulet, R., McCubbrey, D., 1993. Measurement and significance of three-dimensional architecture to the mechanical integrity of trabecular bone. Calcified Tissue International 53, 127 – 133.

Goulet, R.W., Goldstein, S.A., Ciarelli, M.J., Kuhn, J.L., Brown, M.B., Feldkamp, L.A., 1994. The relationship between the structural and orthogonal compressive properties of trabecular bone. Journal of Biomechanics 27, 375 – 389.

Guillén, T., Zhang, Q.H., Tozzi, G., Ohrndorf, a., Christ, H.J., Tong, J., 2011. Compressive behaviour of bovine cancellous bone and bone analogous materials, microCT characterisation and FE analysis. Journal of the mechanical behavior of biomedical materials 4, 1452–61. doi:10.1016/j.jmbbm.2011.05.015.

Hildebrand, T., Rüegesegger, P., 1997. A new method for the model-independent assessment of thickness in three-dimensional images. Journal of Microscopy 185, 67 – 75.

Keaveny, T.M., Morgan, E.F., Niebur, G.L., Yeh, O.C., 2001. Biomechanics of trabecular bone. Annual Review of Biomedical Engineering 3, 307 – 333.

Keaveny, T.M., Pinilla, T.P., Crawford, R.P., Kopperdahl, D.L., Lou, A., 1997. Systematic and random errors in compression testing of trabecular bone. Journal of Orthopaedic Research 15, 101 – 110.

Mirzaali, M.J., Schwiedrzik, J.J., Thaiwichai, S., Best, J.P., Michler, J., Zysset, P.K., Wolfram, U., 2015. Mechanical properties of cortical bone and their relationships with age, gender, composition and microindentation properties in the elderly. Journal of Bone doi:10.1016/j.bone.2015.11.018.

Mottassi, F., Botti, A., Sirleo, L., Carulli, C., Innocenti, M., 2013. Porous metal for orthopedics implants. Clin Cases Miner Bone Metab. 2, 111 – 115.

Otsu, N., 1979. A threshold selection method from grey level histograms. IEEE Transactions on Systems, Man, and Cybernetics 9, 62 – 66.

Patel, M.R., 1969. The deformation and fracture of rigid cellular plastics under multiaxial stress. Ph.D. thesis. University of California, Berkley.

R Development Core Team, 2008. R: A Language and Environment for Statistical Computing. R Foundation for Statistical Computing. Vienna, Austria. URL: `http://www.R-project.org`. ISBN 3-900051-07-0.

Rietbergen, B.v., Odgaard, A., Kabel, J., Huiskes, R., 1998. Relationships between bone mophology and bone elastic properties can be accurately quantified using high-resolution computer reconstructions. Journal of Orthopaedic Research 16, 23 – 28.

Rincón-Kohli, L., 2003. Identification of a multiaxial failure criterion for human trabecular bone. Ph.D. thesis. École Polytechnique Fédérale de Laussanne.

Schoeberl, J., 1997. Netgen, an advancing front 2d/3d-mesh generator based on abstract rules. Computing and Visualization in Science 1, 41 – 52.

Turner, C.H., Cowin, S.C., Rho, J.Y., Ashman, R.B., Rice, J.C., 1990. The fabric dependence of the orthotropic elastic constants of cancellous bone. Journal of Biomechanics 23, 549 – 561.

Wegst, U.G., Bai, H., Saiz, E., Tomsia, A.P., Ritchie, R.O., 2015. Bioinspired structural materials. Nature Materials 14, 23 – 36.

Wolff, J., 1986. The law of bone remodelling. (English Edition) (Berlin: Springer) , 81 – 83.